COMMUNICATIONS IN COMPUTATIONAL PHYSICS
Vol. **3**, No. 1, pp. 33-51

Commun. Comput. Phys.
January 2008

REVIEW ARTICLE

Numerical Modeling of Elastic Wave Propagation in a Fluid-Filled Borehole

Arthur C. H. Cheng[1,*] and Joakim O. Blanch[2]

[1] *Cambridge GeoSciences, 14090 Southwest Freeway, Suite 300, Sugar Land, TX 77478, USA.*
[2] *Nexus GeoSciences, 14090 Southwest Freeway, Suite 240, Sugar Land, TX 77478, USA; previously at SensorWise, Inc., 2908 Rodgerdale, Houston, TX 77042, USA.*

Received 8 March 2007; Accepted (in revised version) 6 June 2007

Available online 14 September 2007

Abstract. We review the methods of simulating elastic wave propagation in a borehole. We considered two different approaches: a quasi-analytic approach using the Discrete Wavenumber Summation Method, and the purely numerical Finite Difference Method. We consider the special geometry of the borehole and discuss the problem in cylindrical coordinates. We point out some numerical difficulties that are particularly unique to this problem in cylindrical coordinates.

AMS subject classifications: 86-08

PACS: 47.11.Bc, 43.35.+d, 91.60.Lj
Key words: Acoustic, borehole, numerical modeling.

Contents

*Corresponding author. *Email addresses:* arthurcheng@alum.mit.edu (A. C. H. Cheng), jblanch@NexusGeo.com (J. O. Blanch)

1 Introduction

Full waveform acoustic logging is a method of obtaining the acoustic properties of the subsurface by lowering a tool into the borehole. The tool generates an acoustic signal inside the fluid-filled borehole. The acoustic wave then propagates in the earth formation around the borehole and is recorded by an array of receivers located on the same tool a short distance away. A schematic diagram of the acoustic logging process is shown in Fig. 1. A detailed description of the process can be found in Tang and Cheng (2004).

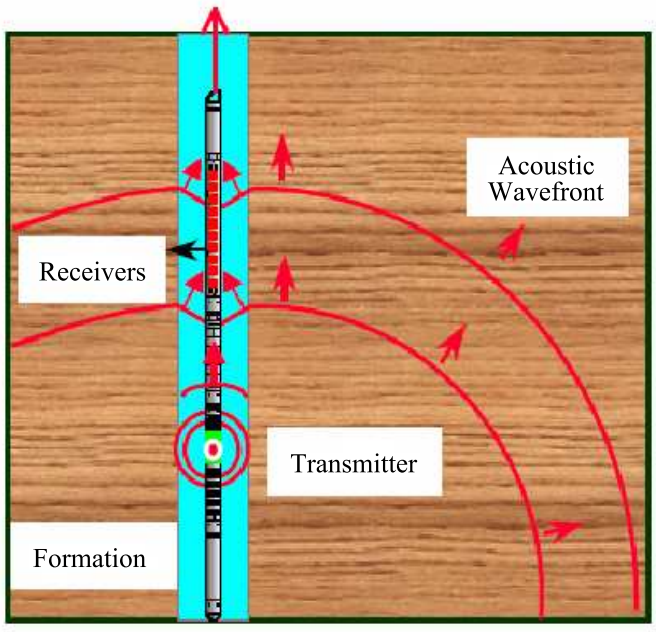

Figure 1: Schematic of the acoustic logging process, from Tang and Cheng (2004).

Because of the particular geometry of the logging process, and the frequencies involved, modeling the acoustic wave propagation is a complex process. In this paper we will describe two frequently used methods for modeling the wave propagation. One is the quasi-analytic method known as the discrete wavenumber summation method, and the other is the finite difference method. We will also discuss other approaches briefly, and the advantages and disadvantages of each under different circumstances.

2 Theory

We will first briefly review the basic analytic formulation of elastic/acoustic wave propagation in a borehole. Let us consider the simple example of a cylindrical borehole of radius R, filled with fluid, in an infinite elastic formation.

The equation of motion is given by:

$$\rho u_{i,tt} = \sigma_{ij,j}, \tag{2.1}$$

where $\vec{u}$ is the displacement vector, ρ the density, and σ is the stress tensor. For an isotropic, elastic solid, we have the generalized Hooke's Law:

$$\sigma_{ij} = \lambda \varepsilon_{ii} \delta_{ij} + 2\mu \varepsilon_{ij}, \tag{2.2}$$

where λ and μ are the Lamé parameters. Assuming a harmonic dependence in time, we can write the wave equation as, applying the relationship between the displacement vector $\vec{u}$ and the strain tensor ε:

$$(\lambda+\mu)\nabla(\nabla\cdot\vec{u}) + \mu\nabla^2\vec{u} + \rho\omega^2\vec{u} = 0, \tag{2.3}$$

where ω is the angular frequency. The displacement vector can be expressed as a combination of a scalar and a vector potential,

$$\vec{u} = \nabla\Phi + \nabla\times(\chi\hat{z}) + \nabla\times\nabla\times(\Gamma\hat{z}) \tag{2.4}$$

where Φ is the compressional-wave potential, $\hat{z}$ is the unit vector in the z-direction (depth), Γ is the SV-type shear-wave potential, and χ is the SH-type shear-wave potential.

In cylindrical coordinates, the ∇^2 operator is given by:

$$\nabla^2 = \frac{\partial^2}{\partial r^2} + \frac{1}{r}\frac{\partial}{\partial r} + \frac{1}{r^2}\frac{\partial^2}{\partial\theta^2} + \frac{\partial^2}{\partial z^2}. \tag{2.5}$$

For a homogenous medium, Eq. (2.3) can be separated into three different equations, each involving a separate potential:

$$\begin{aligned} &\nabla^2\Phi + k_p^2\Phi = 0, \\ &\nabla^2\chi + k_s^2\chi = 0, \\ &\nabla^2\Gamma + k_s^2\Gamma = 0, \end{aligned} \tag{2.6}$$

where $k_p = \omega/\alpha$ and $k_s = \omega/\beta$ are the compressional and shear wavenumbers, and α and β are the compressional and shear velocity, respectively. The general solutions of Eq. (2.6) in the wavenumber-domain are, following the convention of Tang and Cheng (2004):

$$\left.\begin{matrix}\Phi\\ \chi\\ \Gamma\end{matrix}\right\} = e^{ikz}\frac{1}{n!}\left(\frac{fr_0}{2}\right)^2 \begin{cases} (A_nI_n(pr)+B_nK_n(pr))\cos(n(\theta-\phi)), \\ (C_nI_n(pr)+D_nK_n(sr))\sin(n(\theta-\phi)), \\ (E_nI_n(pr)+F_nK_n(sr))\cos(n(\theta-\phi)), \end{cases} \tag{2.7}$$

where r_0 is a constant related to the source, f the radial wavenumber in the fluid, and I_n, K_n are the modified Bessel functions, $p = (k^2 - {k_p}^2)^{1/2}$ and $s = (k^2 - {k_s}^2)^{1/2}$ are the compressional and shear radial wavenumbers, respectively. A, B, C, D, E, and F are

arbitrary constants, and ϕ is an arbitrary reference phase for the source. For a fluid, only the scalar potential exists.

For a borehole, we have a fluid column inside an elastic formation. There are three sets of boundary conditions for wave propagation relating to the acoustic logging environment: 1) the displacements must remain finite at the center of the borehole; 2) there are no incoming waves from infinity; and 3) the stress and displacement continuity across the solid-fluid borehole boundary. In particular for a so-called open borehole, the shear modulus of the fluid inside the borehole vanishes. These conditions put constraints on the type of solutions available. For the Modified Bessel Functions, I_n and K_n, they represent incoming and outgoing waves in cylindrical coordinates, respectively. Thus condition 1 implies that we only have I_n in the inner fluid column, and condition 2 implies that we only have K_n in the outer formation. In addition, we note that K_n is singular at the center ($r=0$, Abramowitz and Stegun, 1964). This, it turns out, will present numerical problems for the Finite Difference Method discussed in a later section. Condition 3 implies that the normal displacement and stress across the borehole boundary are continuous, and the shear stress is zero at the boundary:

$$\begin{cases} u=u_f, \\ \sigma_{rr}=\sigma_{rrf}, \\ \sigma_{rz}=0, \\ \sigma_{r\theta}=0, \end{cases} \qquad (\text{at } r=R) \tag{2.8}$$

where u is the radial component of displacement in the formation, and u_f the radial displacement in the fluid.

3 Synthetic microseismogram and the discrete wavenumber summation method

With the above basic equations, we can calculate the response inside the borehole from a point source excitation. In general, the response can be written as (Tang and Cheng, 2004):

$$P(z,t)=\int_{-\infty}^{\infty} S(\omega)D^{(0)}(\omega)e^{-i\omega t}d\omega+\int_{-\infty}^{\infty}\int_{-\infty}^{\infty} S(\omega)A_0'(k,\omega)e^{ikz}e^{-i\omega t}dkd\omega, \tag{3.1}$$

where P is the pressure response at a distance z along the borehole axis from the source and $S(\omega)$ is the source spectrum. The first integral relates to the direct signature of the source, and the second integral is the response of the borehole to the source excitation. The first term can easily be calculated using a standard analytic solution of wave propagating in a homogeneous fluid. It is the second term that we will need to focus our attention on.

We can calculate the second integral, specifically the wavenumber integral inside the frequency integral, using the discrete wavenumber summation method (Bouchon and

Aki, 1977, Cheng and Toksöz, 1981). There are two issues involved in the numerical evaluation of the wavenumber integral. The first one is that the summation is along the real wavenumber k axis. The response term A_0' has singularities lying along the real k axis. These are branch points corresponding to the compressional and shear head wave arrivals, and poles corresponding to the guided (pseudo-Rayleigh and Stoneley, or trapped waves and interface waves for orders higher than zero) wave arrivals (Tsang and Radar, 1979; Cheng and Toksöz, 1981, Paillet and Cheng, 1991). The second issue involves the discretization interval for the numerical integration over the wavenumber.

The solution to the first part is to distort the path of integration by the use of complex frequencies, adding in a small imagery part ω_i to the real frequencies (Bouchon and Aki, 1977, Cheng and Toksöz, 1981). This has the effect of moving the singularities off the real k axis in the complex k plane. This also has an effect of attenuating later arrivals. This attenuating effect is reversed by multiplying the calculated response by $exp(\omega_i t)$. It is useful to note at this point that one should not use a large value of ω_i, otherwise numerical noise in the late part of the waveform will be magnified. An additional method of moving the singularities off the real k axis is the use of attenuation in the formation and fluid velocities. Attenuation is usually formulated by using a complex velocity instead of a purely real velocity formulation (Aki and Richards, 1980). It is also necessary to ensure that the complex velocity follows the Kramer-Krönig's relation, such that the wavefield is causal and hence realistic.

For the discretization of the wavenumber integral, it is observed that analogous to the time-frequency pair in the Fourier Transform, space-wavenumber also form a Fourier Transform pair. Thus a discretization in wavenumber implies a periodicity in space. Specifically,

$$\Delta k = 2\pi / L, \tag{3.2}$$

where L is the periodicity in space. We will have to choose a Δk such that L is large enough that arrivals from the nearest periodic sources will not interfere with our calculated waveform.

The above is the description of the application of the discrete wavenumber summation method to model elastic wave propagation in a borehole. This technique can be generalized to calculate the response in a borehole with radial layers (Tubman et al., 1984, Schmitt et al., 1988), a transversely isotropic borehole with the axis of symmetry coinciding with the axis of the borehole (Schmitt, 1989), a permeable borehole (Schmitt et al., 1988), a borehole with an irregular boundary (Bouchon and Schmitt, 1989), and the responses of off-centered sources and receivers (Byun and Toksöz, 2006). It is limited to situations where the formation properties are homogeneous in the z and θ directions. For more complex formations, we need to use the finite difference technique to model the response.

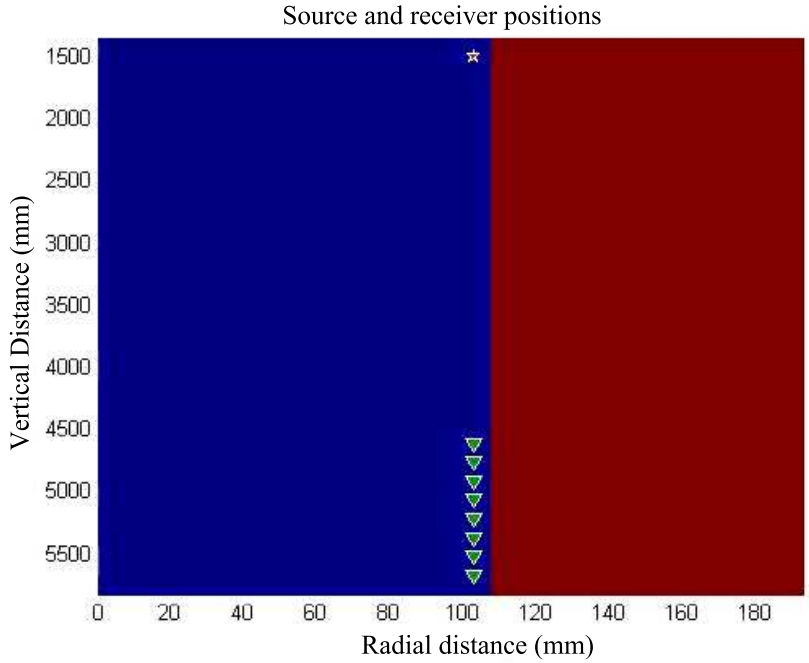

Figure 2: A red star denotes the source and the receivers are denoted by green triangles. The blue area corresponds to mud, and red the formation. Note that the scale is very different between the radial distance and depth/vertical distance. The receiver configuration is similar to a typical wireline acoustic tool, except that two of the receiver arrays are located within the formation. The scales are in number of grid points.

4 The finite difference method

When one wants to simulate the wave propagation in a borehole with no cylindrical symmetry or with variations in the vertical (z) direction, it is no longer possible to efficiently use the discrete wavenumber method, but necessary to use the Finite Difference method or another method which can solve a general system of partial differential equations. For a completely heterogeneous borehole, the most efficient method is to do the simulation in three dimensions and in Cartesian coordinates. Cheng et al. (1995) describes the procedure of such a simulation. There are obvious limitations to such an approach, and the approximation of the curved surface of the borehole in a Cartesian coordinate system is one. These limitations are quite well understood and beyond the scope of this paper.

In this paper, we would like to address a different problem, namely, a radially and vertically heterogeneous borehole when we can apply the Finite Difference method in 2 dimensions in cylindrical coordinates (r and z). The angular dependence can be prescribed by deriving the 2D cylindrical equation using a function, which is the product of one function depending on both r and z, and another depending only on the angle, $u=u(r,z)\Theta(\theta)$. To maintain consistency in angular behavior the solutions for the angular

behavior are the well-known discrete spectra sinusoids. It is, however, not possible to eliminate one set of solutions as outlined above in the discussion about boundary conditions.

For the Finite Difference Method, we used a different approach to solving the elastic wave equation (2.1). Instead of the use of potentials, and looking for a time harmonic solution, the elastic wave equation is obtained by first deriving the strain in cylindrical coordinates and then using the constitutive relation for linear elasticity to express the stress using the derivatives of the displacement. The slight complication in the derivation is that care has to be taken of the non-constant coordinate direction vectors, which are dependent on the angle (see Eq. (2.5)). Adding Newton's second law to the stress and using the particle velocity $\vec{v}=\vec{u}_{,t}$ instead of the displacement $\vec{u}$ completes the derivation.

$$\begin{cases} \sigma_{rr,t}=(\lambda+2\mu)v_{r,r}+\lambda\left(\frac{1}{r}v_r+n\frac{1}{r}v_\theta+v_{z,z}\right), \\ \sigma_{\theta\theta,t}=(\lambda+2\mu)\left(\frac{1}{r}v_r+n\frac{1}{r}v_\theta\right)+\lambda(v_{r,r}+v_{z,z}), \\ \sigma_{zz,t}=(\lambda+2\mu)v_{z,z}+\lambda\left(v_{r,r}+\frac{1}{r}v_r+n\frac{1}{r}v_\theta\right), \\ \sigma_{rz,t}=\mu(v_{r,z}+v_{z,r}), \\ \sigma_{r\theta,t}=\mu\left(v_{\theta,r}-n\frac{1}{r}v_r-\frac{1}{r}v_\theta\right), \\ \sigma_{\theta z,t}=\mu\left(v_{\theta,z}-n\frac{1}{r}v_z\right), \\ v_{r,t}=\frac{1}{\rho}\left(\frac{1}{r}\sigma_{rr}+\sigma_{rr,r}+n\frac{1}{r}\sigma_{r\theta}-\frac{1}{r}\sigma_{\theta\theta}+\sigma_{rz,z}\right), \\ v_{\theta,t}=\frac{1}{\rho}\left(\frac{2}{r}\sigma_{r\theta}+\sigma_{r\theta,r}-n\frac{1}{r}\sigma_{\theta\theta}+\sigma_{\theta z,z}\right), \\ v_{z,t}=\frac{1}{\rho}\left(\frac{1}{r}\sigma_{rz}+\sigma_{rz,r}+n\frac{1}{r}\sigma_{\theta z}+\sigma_{zz,z}\right). \end{cases} \tag{4.1}$$

The angular dependencies are simple sinusoids with frequency n. There is a phase shift between the different components, such that if the angular dependence for the v_θ, $\sigma_{r\theta}$, and $\sigma_{\theta z}$ is $\sin(n\theta)$, the angular dependence for the others are $\cos(n\theta)$. Note that if the order of the solutions n is equal to zero ($n=0\Leftrightarrow$ monopole), the equations decouple, such that the angular components, which would correspond to an SH wave in Cartesian coordinate system, decouple from the other radial and axial/depth (z) components.

The system of equations (4.1) can, as mentioned above, be solved using the Finite Difference method. However, due to the existence of a singular solution in the fluid column, the problem is not well posed (Gustafsson et al., 1995). Thus, if small round-off errors in the Finite Difference solution correspond to the solution K_n, which is singular at the center of the borehole, this solution will be picked up and cause uncontrollable growth of the computed solution. This situation does not exist for the Discrete Wavenumber Summation method above since we can analytically eliminate that solution. Still, there are

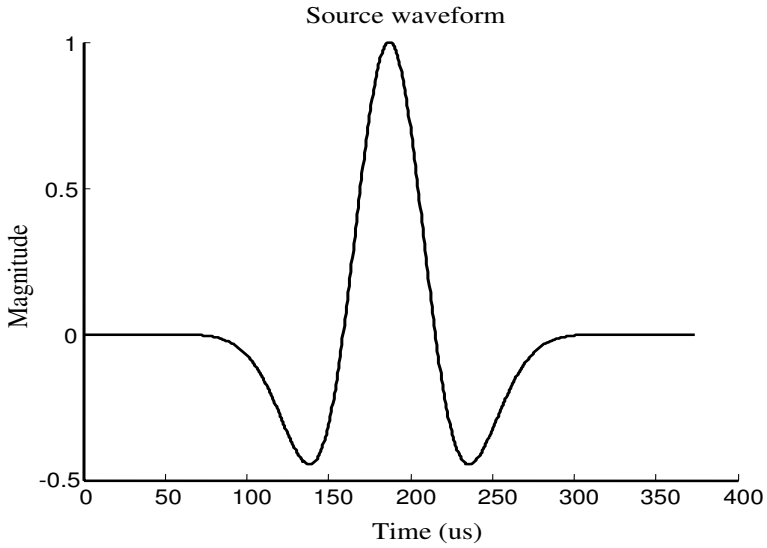

Figure 3: The source wavelet used in all simulations, which is a Ricker wavelet (i.e., second derivative of a Gaussian) with a center frequency of 8 kHz.

cases where a useful solution can be obtained. In the following sections we will show examples where the Finite Difference Method produces a useful solution and where it fails. The Finite Difference employed here is second order accurate in time and fourth order accurate in space (Robertsson et al., 1994). The source is a pure pressure source in the fluid column of the borehole, and field is measured as pressure both in the fluid and the formation (the trace of the stress tensor).

5 Open borehole example

Fig. 2 shows an open borehole scenario with fluid and a formation and positions of sources and receivers. The spatial step is 5 mm in both the radial direction and depth, and the time step is 0.5 μs. The borehole is filled with mud (200 μs/ft) and the formation has a compressional slowness of 100 μs/ft and a shear slowness of 170 μs/ft. The density is 1.1 gcm^3 in the mud and 2.2 g/cm^3 in the formation. For all simulations in this paper, we use a Ricker wavelet with a center frequency of 8 kHz (see Fig. 3). The upper, lower, and right sides of the model contain absorbing sponge boundaries (Robertsson et al., 1994). For reference, at a center frequency of 8 kHz, a compressional wave wavelength is approximately 400 mm in the formation.

Figs. 4-10 show the solution for $n=0,1,2$, commonly known as monopole, dipole, and quadrupole source pattern, with the receiver array in the fluid. The source is an 8 kHz Ricker wavelet displayed in Fig. 3. Fig. 4 shows the eight receiver waveforms for the $n=0$ monopole source, the spectra for the receivers, the energy stack, the slowness-time

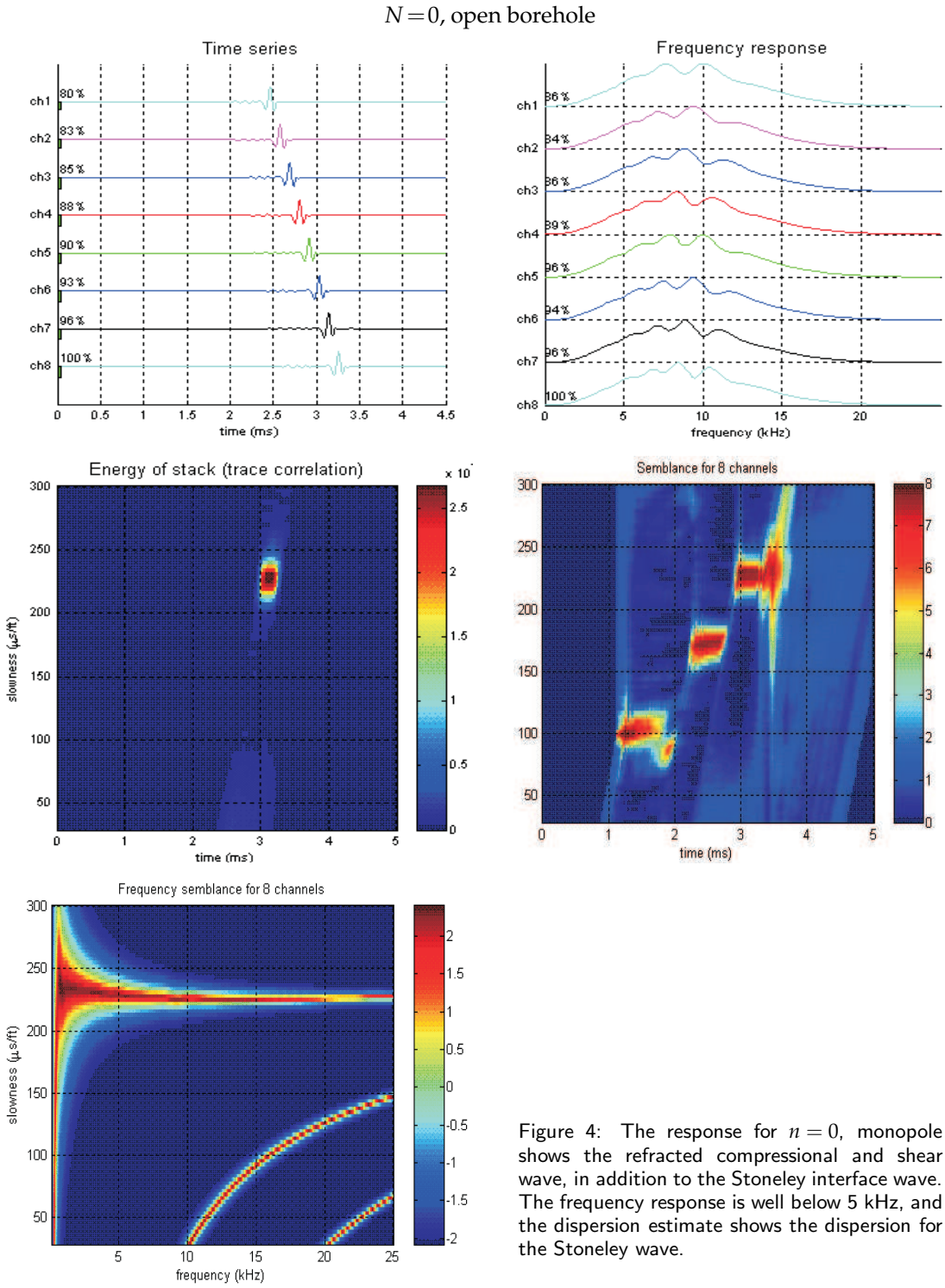

Figure 4: The response for $n=0$, monopole shows the refracted compressional and shear wave, in addition to the Stoneley interface wave. The frequency response is well below 5 kHz, and the dispersion estimate shows the dispersion for the Stoneley wave.

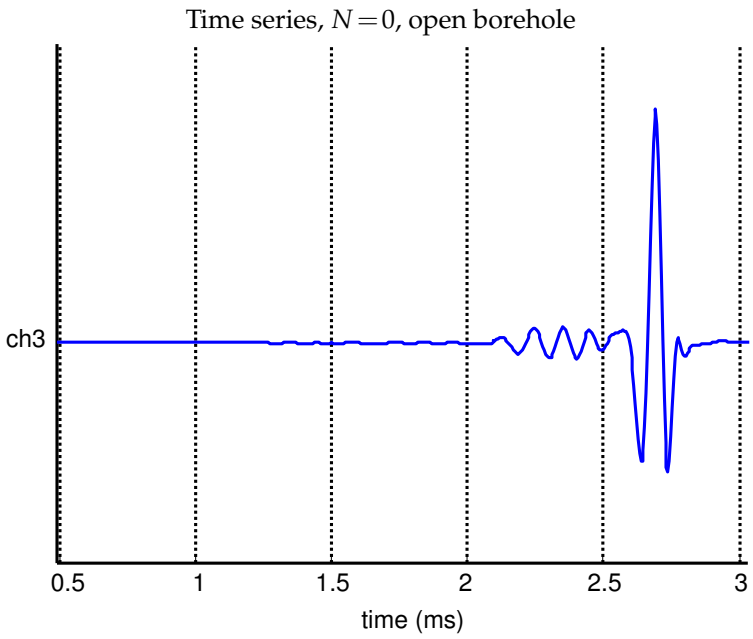

Figure 5: The response from channel 3 for a monopole source shows that most of the energy is carried in the Stoneley wave, there is a hint of the compressional (marked) and shear wave arrival. The time scale is in milliseconds.

semblance coherence (Kimball and Marzetta, 1986), and the slowness dispersion from frequency semblance across the receiver array. We can see the refracted compressional and shear arrivals, in addition to the interface guided (pseudo-Rayleigh and Stoneley) waves (see, e.g., Tang and Cheng, 2004, for a complete description of these waves, as well as the flexural and screw modes, generated by the dipole and quadrupole excitations, respectively). Fig. 5 shows a close up view of one of the waveforms. As can be seen from the figure, most of the energy is carried in the interface waves, with only a hint visible of the refracted compressional and shear head wave arrivals.

Figs. 6 and 7 show the response for an $n=1$, or dipole source. There are refracted compressional and shear wave arrivals, in addition to the flexural interface wave. The dipole source pattern clearly excites more high frequencies than the monopole source. This is because of the low frequency cutoff for the flexural mode. Figs. 8 and 9 show the results for a quadrupole ($n=2$) source. As predicted by the theory, the quadrupole mode contains higher frequencies than both the Stoneley and the flexural mode. The refracted compressional head wave is more visible because of the reduced amplitude of the interface modes when compared to the monopole and dipole excitations.

Fig. 10 shows the same waveform as Fig. 9, except on an extended time axis. This is to demonstrate that the finite difference simulations in these cases appear to be stable, despite the theoretical presence of the singular solution in the fluid.

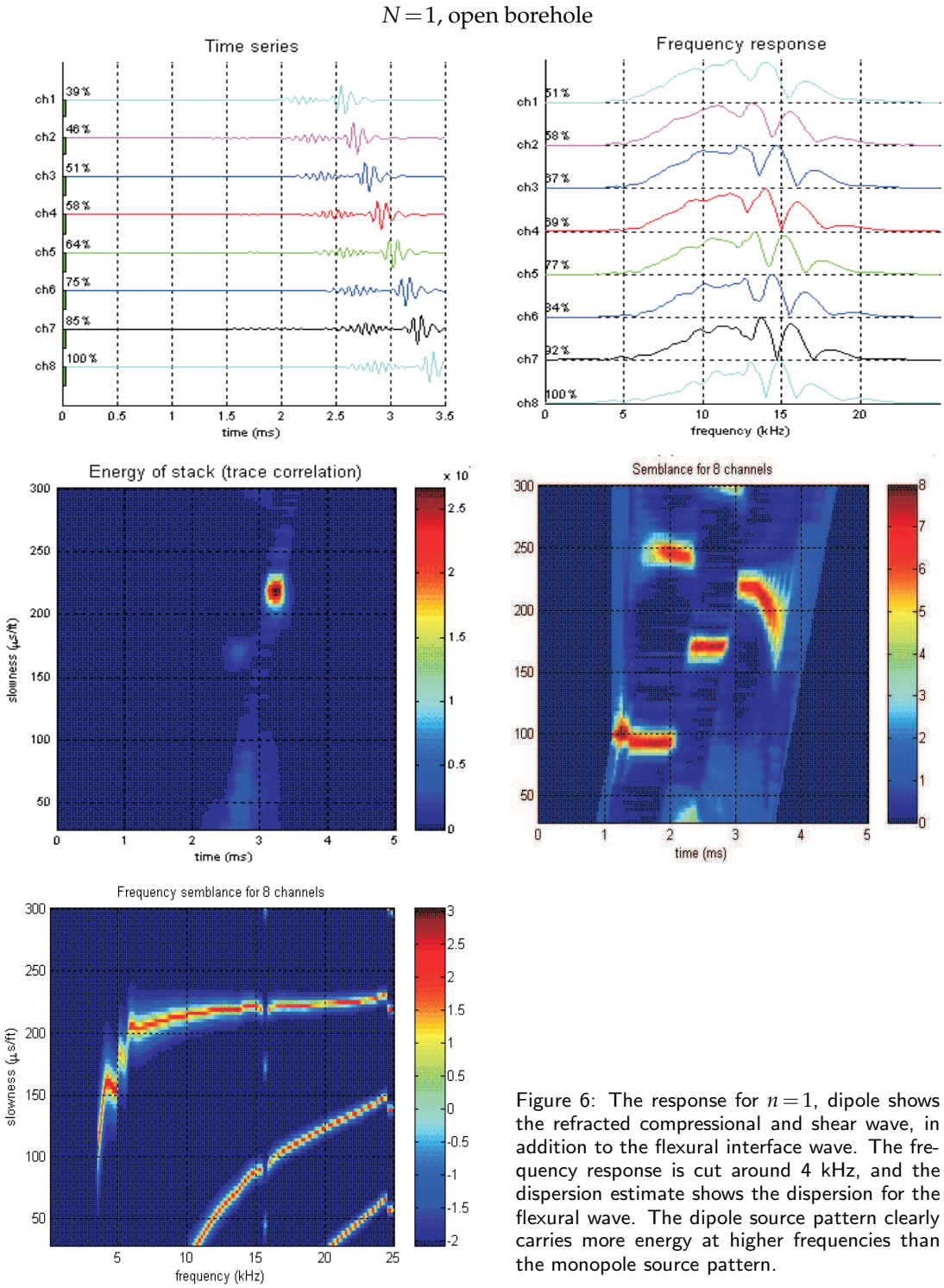

Figure 6: The response for $n=1$, dipole shows the refracted compressional and shear wave, in addition to the flexural interface wave. The frequency response is cut around 4 kHz, and the dispersion estimate shows the dispersion for the flexural wave. The dipole source pattern clearly carries more energy at higher frequencies than the monopole source pattern.

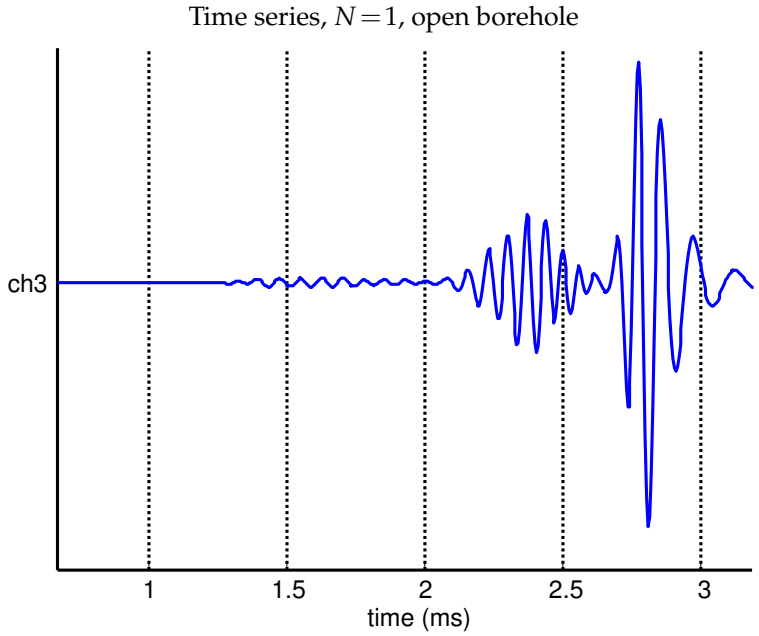

Figure 7: The response from channel 3 for a dipole source shows that most of the energy is carried in the flexural wave, there is a hint of the compressional arrival (marked) but the shear wave carries a significant part of the energy as well. The time scale is in milliseconds.

6 Borehole with logging tool

We will now examine a more realistic situation, namely, one with a logging tool in the middle of the borehole. We simulate the logging tool by placing a steel body at the center of the borehole, with high attenuation streaks corresponding to similar material in an actual tool, whose purpose is to damp out the direct arrival of the acoustic wave through the tool body. Fig. 11 is a schematic of the simulation grid.

Figs. 12 and 13 show the waveform from a monopole simulation. The results are similar to those in Fig. 4, without a steel tool, in that the pseudo-Rayleigh and Stoneley waves dominate the waveform, but the effect of the steel tool is evident. The solution is still stable within the time frame of the simulation.

Fig. 14 shows the waveform from channel 3 of the wavefield under dipole source excitation. In this case the singular solution, K_n, is picked up, and the simulation becomes unstable. When we look further into the waveforms and analyze them using the slowness-time semblance correlation (Kimball and Marzetta, 1986) shown in Fig. 15, we can detected that there is some time before the solution is corrupted and overtaken by the singular solution. Part of the compressional wave has arrived and is visible in the slowness-time coherence plot. We can attempt to eliminate the singular solution by setting the fields around the origin to zero, thus delaying the time for the singular solution to develop. Fig. 16 shows the slowness-time coherence plot shows that this approach works to some extent, and we do pick up the dipole flexural wave arrival.

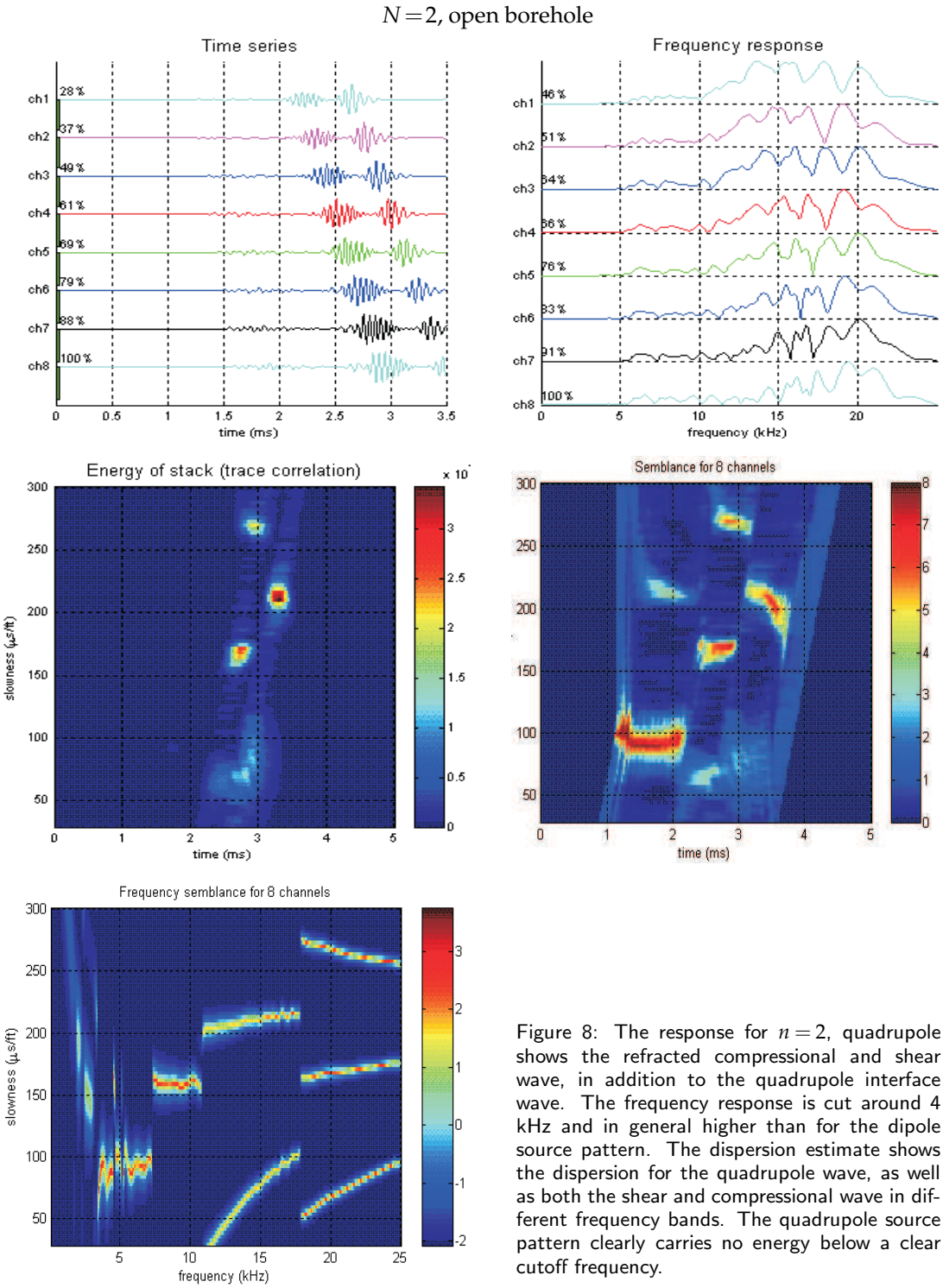

Figure 8: The response for $n=2$, quadrupole shows the refracted compressional and shear wave, in addition to the quadrupole interface wave. The frequency response is cut around 4 kHz and in general higher than for the dipole source pattern. The dispersion estimate shows the dispersion for the quadrupole wave, as well as both the shear and compressional wave in different frequency bands. The quadrupole source pattern clearly carries no energy below a clear cutoff frequency.

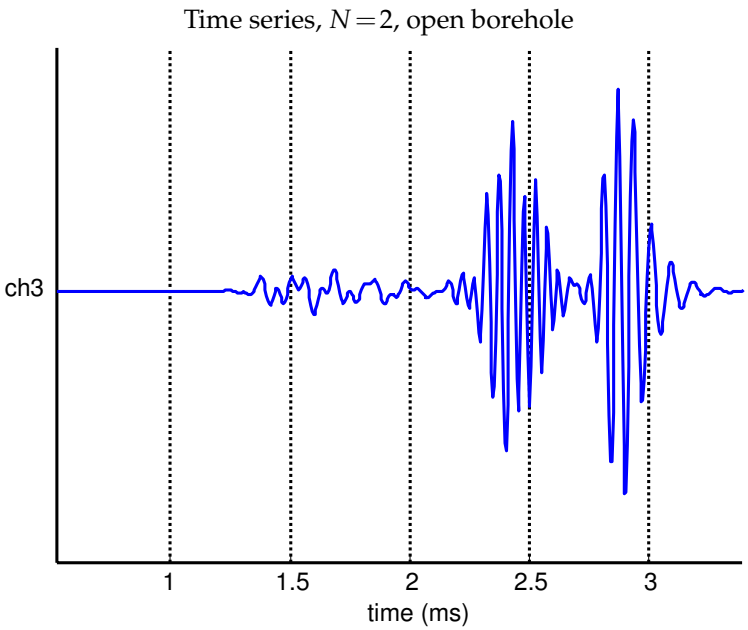

Figure 9: The response from channel 3 for a quadrupole source shows that about an equal amount of energy is carried in the shear and quadrupole wave. The compressional arrival (marked) is clearly visible. The time scale is in milliseconds.

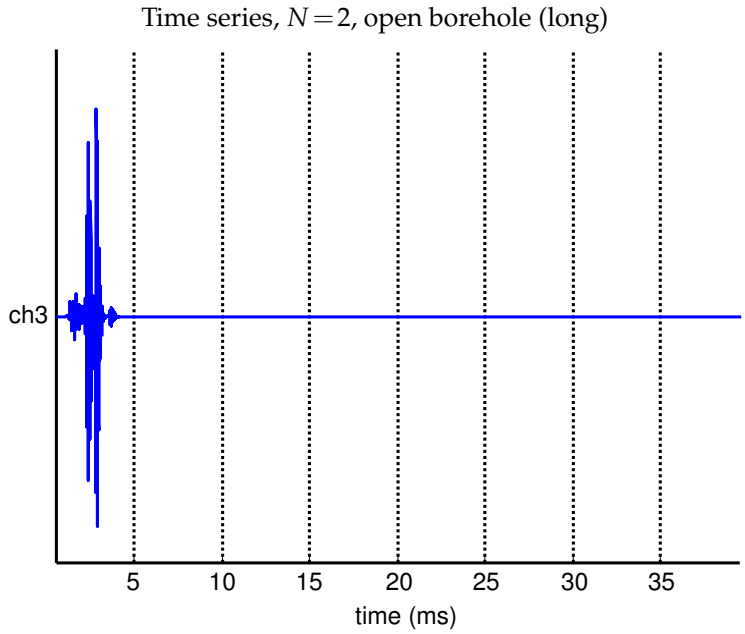

Figure 10: The same data as in Fig. 9, but with an extended time axis. The FD solution seems to be stable (as well as good absorbing boundaries). The time scale is in milliseconds.

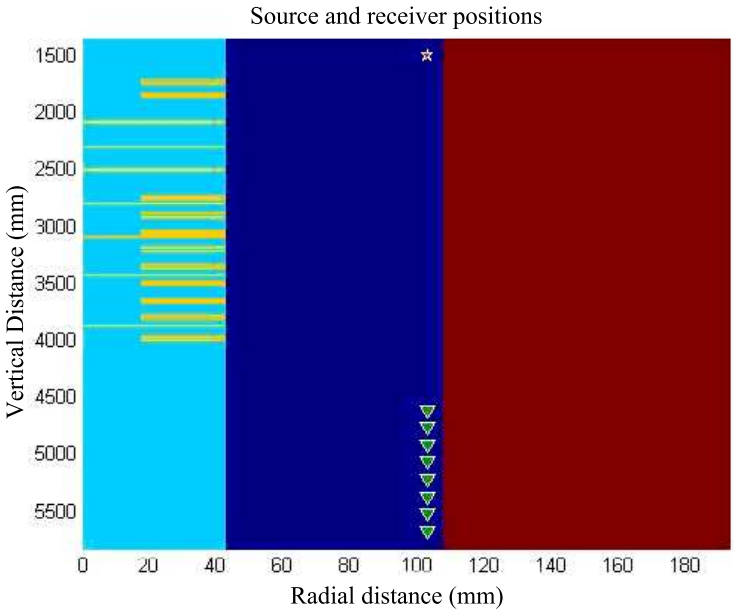

Figure 11: A red star denotes the source and the receivers are denoted by green triangles. Note that the scale is very different between the radial distance and depth/vertical distance. The blue color represents borehole fluid, the red formation, and the cyan the steel tool body. The yellow stripes are section with high attenuation. The receiver configuration is the same as in Fig. 2. The scales are in number of grid points.

Even, though the simulation is unstable for all cases since the formulation is not well-posed as pointed out above it is worth spending some time trying to understand why the stability problem starts to appear earlier with the dipole excitation combined with a steel tool in the center of the borehole. There are a number of reasons why this is so. In a fluid, we only have the scalar potential, and the singular solution associated with that is K_0. Even though for the higher order excitation, the solution involves derivatives of K_0, K_0 is a logarithmic singularity at the center of the borehole, and thus the unstable solution grows slowly. In a steel tool body, we have both the scalar and vector potential as discussed above, the solution associated with the vector potential, the shear wave solution, is of the order K_{n+1}, where n is the order of excitation of the source. Thus for dipole or $n=1$ excitation, the singular solution is proportional to K_2. K_2 approaches infinity as $1/z^2$ as z approaches 0, much faster than logarithmically (Abramowitz and Stegun, 1964). Thus we have problems when we do simulations of a borehole with a solid steel tool body in the center, with a dipole and higher order sources.

7 Summary

We have presented a brief review of two standard methods of numerical simulation of elastic wave propagation in a borehole. The Discrete Wavenumber Summation Method

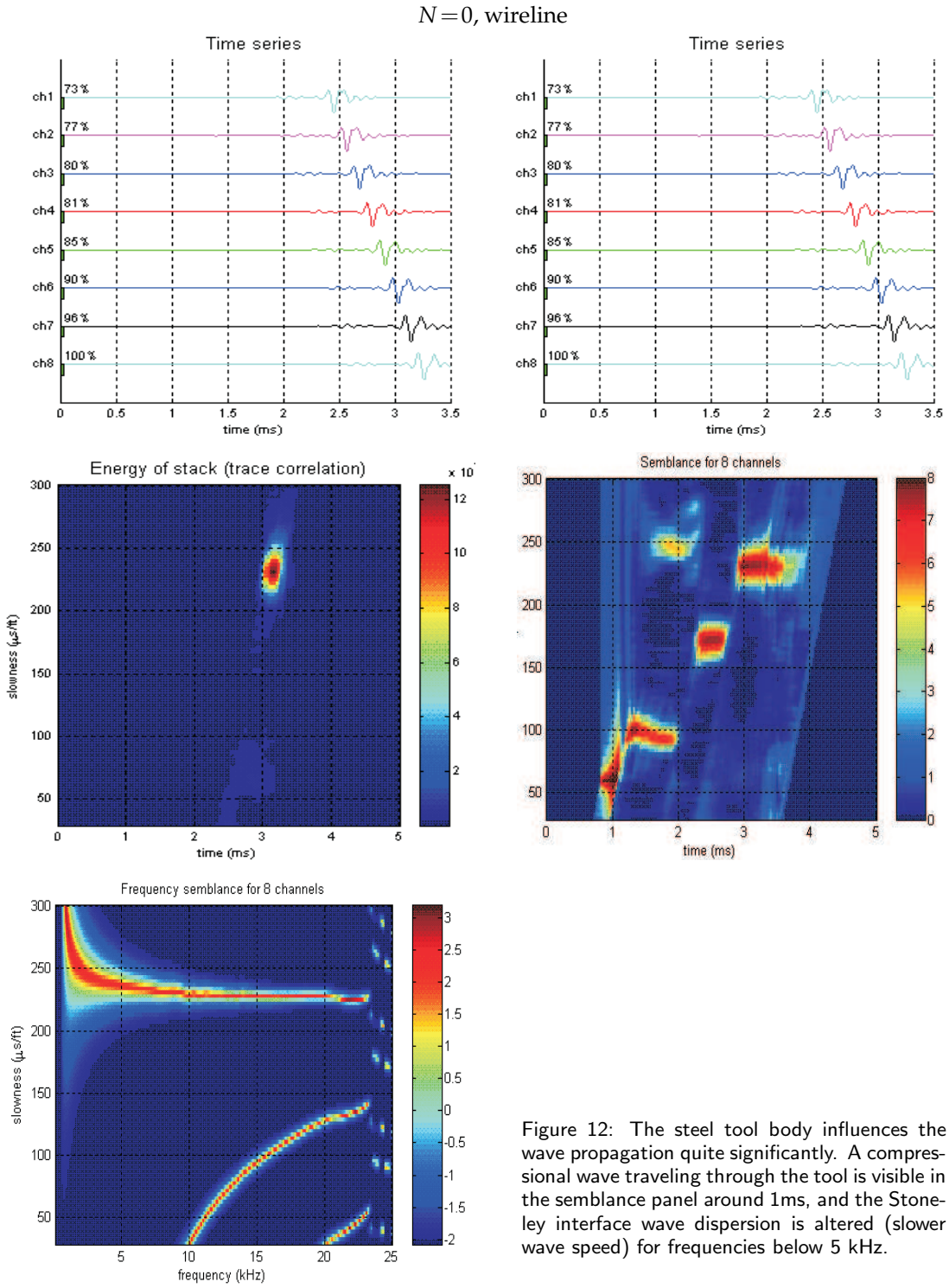

Figure 12: The steel tool body influences the wave propagation quite significantly. A compressional wave traveling through the tool is visible in the semblance panel around 1ms, and the Stoneley interface wave dispersion is altered (slower wave speed) for frequencies below 5 kHz.

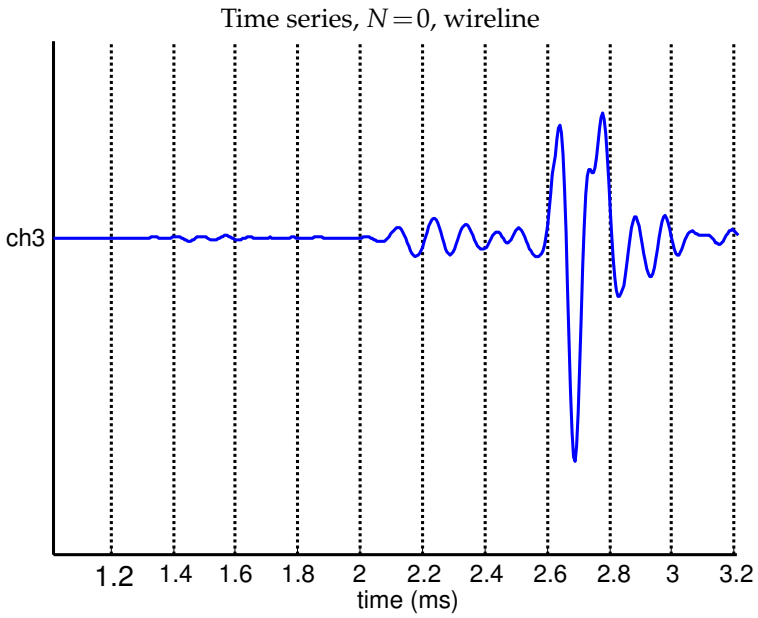

Figure 13: The response from channel 3 for a monopole source and a steel tool shows that most of the energy is carried in the Stoneley wave. The polarity of the Stoneley wave is different compared to the open borehole case due to different dispersion and source coupling. The time scale is in milliseconds.

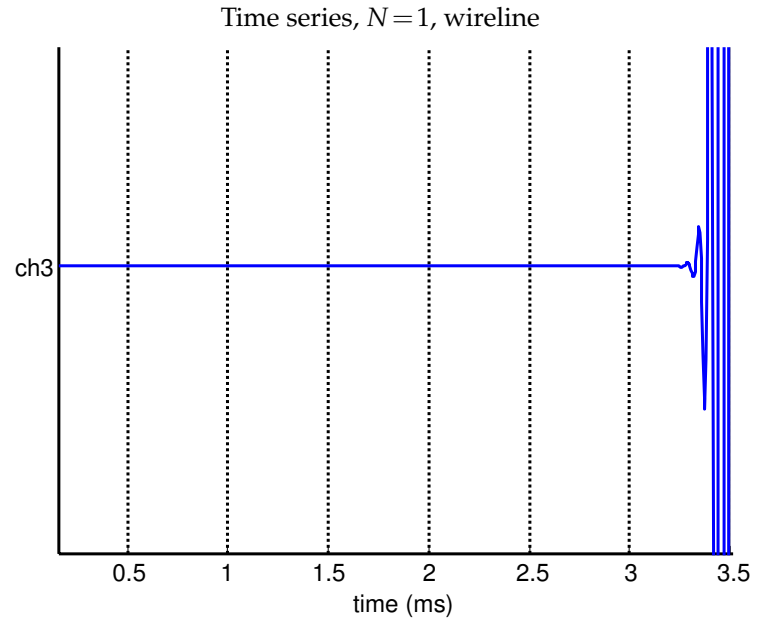

Figure 14: The response from channel 3 for a dipole source and a steel tool shows that the simulation is unstable. In this case the singular solution is picked up. The time scale is in milliseconds.

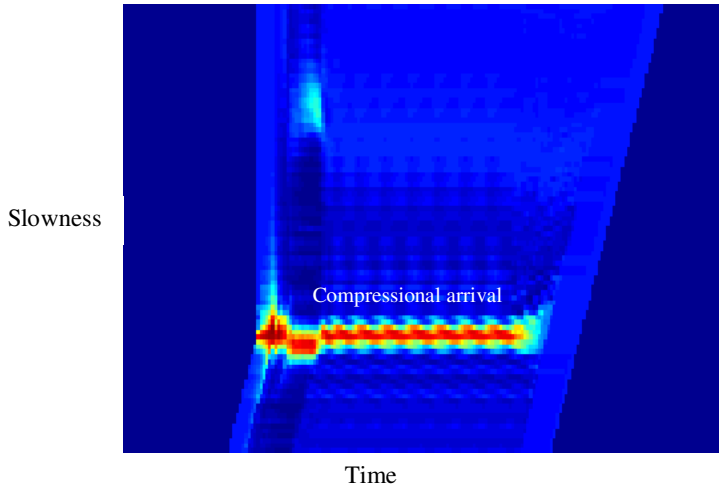

Figure 15: The semblance for the steel tool, $n=1$, data shows that there is some time before the solution is overtaken by the singular solution. Part of the compressional wave has arrived before the solution is corrupted.

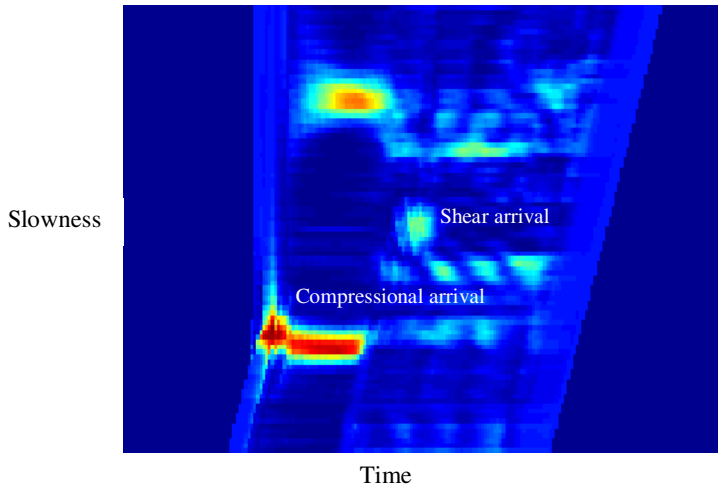

Figure 16: In an attempt to force the solution to not become corrupted by setting the fields around the origin to zero, the time for the singular solution to develop is delayed. The semblance for the steel tool, $n=1$, data shows that there is some time before the solution is overtaken by the singular solution. Here it is possible to conclude that the $n=1$, dipole source pattern suppresses the tool mode.

is quasi-analytic, but is limited to situations with radial symmetry and homogeneous formation in the vertical direction. The 2D Finite Difference Method offers a solution for a radially and vertically heterogeneous borehole, but is limited by numerical instabilities when high order excitation is introduced together with a solid logging tool in the center of the borehole.

References

[1] M. Abramowitz and I. A. Stegun (Eds.), Handbook of Mathematical Functions, Dover, 1964.
[2] K. Aki and P. G. Richards, Quantitative Seismology: Theory and Methods, W. H. Freeman and Co., 1980.
[3] M. Bouchon and K. Aki, Discrete wavenumber representation of seismic-source wavefields, SSA Bull., 67 (1977), 259-277.
[4] M. Bouchon and D. P. Schmitt, Full-wave acoustic logging in an irregular borehole, Geophysics, 54(6) (1989), 758-765.
[5] J. Byun and M. N.Toksöz, Effects of an off-centered tool on dipole and quadrupole logging, Geophysics, 71(4) (2006), F91-F100.
[6] C. H. Cheng and M. N. Toksöz, Elastic wave propagation in a fluid-filled borehole and synthetic acoustic logs, Geophysics, 56 (1981), 1603-1613.
[7] N. Y. Cheng, C. H. Cheng and M. N. Toksöz, Borehole wave propagation in three dimensions, J. Acoust. Soc. Am., 84 (1995), 2215-2229.
[8] B. Gustafsson, H.-O. Kreiss and J. Oliger, Time Dependent Problems and Difference Methods, Wiley, 1995.
[9] C. V. Kimball and T. L. Marzetta, Semblance processing of borehole acoustic array data, Geophysics, 49 (1986), 274-281.
[10] F. L. Paillet and C. H. Cheng, Acoustic Waves in Boreholes, CRC press, 1991.
[11] J. O. A. Robertsson, J. O. Blanch and W. W. Symes, Viscoelastic finite-difference modeling, Geophysics, 59 (1994), 1444-1456.
[12] D. P. Schmitt, Acoustic multipole logging in transversely isotropic poroelastic formations, J. Acoust. Soc. Am., 86 (1989), 2397-2421.
[13] D. P. Schmitt, M. Bouchon and G. Bonnet, Full-waveform synthetic acoustic logs, in radially semi-infinite saturated porous formations, Geophysics, 53 (1988), 807-823.
[14] X. M. Tang and A. C. H. Cheng, Quantitative Acoustic Logging Methods, Elsevier, 2004.
[15] L. Tsang and D. Radar, Numerical evaluation of the transient acoustic waveform due to a point source in a fluid-filled borehole, Geophysics, 44 (1979), 1706-1720.
[16] K. Tubman, C. H. Cheng and M. N. Toksöz, Synthetic full waveform acoustic logs in cased boreholes, Geophysics, 49(7) (1984), 1051-1059.